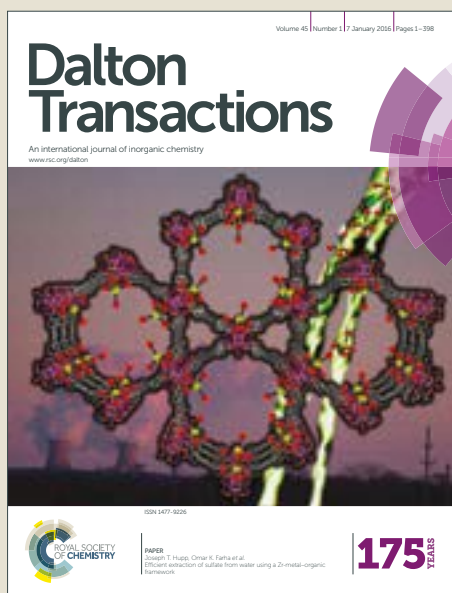


# Dalton Transactions

Accepted Manuscript



This article can be cited before page numbers have been issued, to do this please use: S. Telukutla, S. Privér, V. V. Rao, N. Mirzadeh and S. K. Bhargava, *Dalton Trans.*, 2018, DOI: 10.1039/C8DT01724G.



This is an Accepted Manuscript, which has been through the Royal Society of Chemistry peer review process and has been accepted for publication.

Accepted Manuscripts are published online shortly after acceptance, before technical editing, formatting and proof reading. Using this free service, authors can make their results available to the community, in citable form, before we publish the edited article. We will replace this Accepted Manuscript with the edited and formatted Advance Article as soon as it is available.

You can find more information about Accepted Manuscripts in the [author guidelines](#).

Please note that technical editing may introduce minor changes to the text and/or graphics, which may alter content. The journal's standard [Terms & Conditions](#) and the ethical guidelines, outlined in our [author and reviewer resource centre](#), still apply. In no event shall the Royal Society of Chemistry be held responsible for any errors or omissions in this Accepted Manuscript or any consequences arising from the use of any information it contains.



## ARTICLE

## Gold(I) and Gold(III) Phosphine Complexes: Synthesis, Anticancer Activities Towards 2D and 3D Cancer Models, and Apoptosis Inducing Properties

Received 00th January 20xx,  
Accepted 00th January 20xx

DOI: 10.1039/x0xx00000x

www.rsc.org/

T. Srinivasa Reddy, Steven H. Privér, Vijay V. Rao, Nedaossadat Mirzadeh,\* Suresh K. Bhargava\*

A series of gold(I), gold(III) and cationic gold(I) complexes of tris(4-methoxyphenyl)phosphine and tris(2,6-dimethoxyphenyl)phosphine were synthesized and fully characterized by spectroscopic methods. The molecular structures of selected complexes were also determined by X-ray diffraction analysis. The prepared complexes [AuX{P(C<sub>6</sub>H<sub>4</sub>-4-OMe)<sub>3</sub>}] [X = Cl (**1**), Br (**2**), I (**3**)], [AuCl<sub>3</sub>{P(C<sub>6</sub>H<sub>4</sub>-4-OMe)<sub>3</sub>}] (**4**), [Au{P(C<sub>6</sub>H<sub>4</sub>-4-OMe)<sub>3</sub>}<sub>2</sub>]PF<sub>6</sub> (**5**), [AuX{P(C<sub>6</sub>H<sub>3</sub>-2,6-{OMe}<sub>2</sub>)<sub>3</sub>}] [X = Cl (**6**), Br (**7**), I (**8**)], [AuCl<sub>3</sub>{P(C<sub>6</sub>H<sub>3</sub>-2,6-{OMe}<sub>2</sub>)<sub>3</sub>}] (**9**) and [Au{P(C<sub>6</sub>H<sub>3</sub>-2,6-{OMe}<sub>2</sub>)<sub>3</sub>}<sub>2</sub>]PF<sub>6</sub> (**10**) were investigated for their anticancer activity against five human tumor cell lines [ovarian (SKOV-3), fibrosarcoma (HT1080), glioblastoma (U87MG), prostate (PC-3), cervical (HeLa)] as well as in 3D spheroidal models of HeLa cells. The cationic complex **10** was found to exhibit a remarkably broad spectrum of anticancer activity with approximately 30 fold higher toxicity than cisplatin against PC-3 and U87MG cancer cells; this complex also showed the strongest inhibition of spheroid growth in 3D models of HeLa cells. The mechanism of anticancer activity of these gold complexes was found to be strong inhibition of thioredoxin reductase, increased ROS production and subsequent apoptosis induction as evidenced by the sub G1 cell accumulation, DNA fragmentation, and caspase-3 activation.

### Introduction

Gold phosphine complexes are ubiquitous in gold chemistry, and they continue to be the subject of considerable intrigue owing to their wide spectrum of anticancer properties.<sup>1-6</sup> Since the discovery that auranofin, the first clinically approved gold phosphine drug for the treatment of rheumatoid arthritis,<sup>7-8</sup> also possessed potent *in vitro* anticancer activities,<sup>9</sup> there has been growing interest in developing gold(I) phosphine complexes of the type [AuX(PR<sub>3</sub>)] (X = halogen, thiolate; R = alkyl, aryl). Recent reports on the anticancer properties of triphenylphosphine gold chloride, [AuCl(PPh<sub>3</sub>)], and its ability to induce autophagy has offered greater insights into the biological properties of this class of gold complex.<sup>10</sup> These gold(I) phosphines appear to selectively accumulate in mitochondria, which represent the most likely site for their biological action. Further, gold complexes, including auranofin, proposed to induce apoptosis by increasing free radical formation *via* inhibition of the mitochondrial isoform of thioredoxin reductase.<sup>11-14</sup>

To develop gold phosphine drugs, an important factor to consider is the lipophilicity of the compound, since this plays a significant role in cellular uptake, intracellular biodistribution, and pharmacokinetic properties.<sup>15,16</sup> It has been shown that highly lipophilic gold(I) phosphine complexes display remarkable anticancer properties, however, they also exhibit severe toxicity to healthy normal tissues.<sup>17</sup> One way to increase the bio-distribution and selectivity for

tumor tissue is by increasing the hydrophilic to lipophilic ratio of the complex. This ratio can be altered by careful ligand design. Since the influence of the phosphine ligand in terms of the cytotoxic properties of phosphine-containing gold complexes is still not clear, we chose to investigate what the effect of methoxy substituents on the phosphine backbone would have on the anticancer activity of a range of gold complexes. Recent reports on gold(I) and gold(III) derivatives of the 2-(2'-pyridyl)benzimidazole (pbiH) ligand enabled the exploration of different oxidation states of gold on anticancer activity.<sup>18,19</sup>

Herein, we report the synthesis of a number of gold(I) and gold(III) complexes containing methoxy-substituted triaryl phosphine ligands. The anticancer properties of the prepared complexes (shown in Fig. 1) have been explored towards a wide range of cancer cells, and the mechanism of cell death was investigated in HeLa cancer cells.

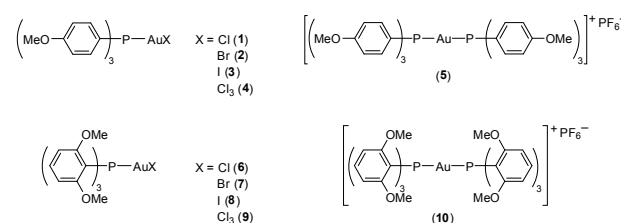


**Fig. 1** Structures of the gold complexes containing methoxy-substituted triaryl phosphine ligands used in this investigation.

Centre for Advanced Materials & Industrial Chemistry (CAMIC), School of Science,  
RMIT University, GPO Box 2476, Melbourne 3001, Australia

E-mail: Suresh.Bhargava@rmit.edu.au

Electronic Supplementary Information (ESI) available: See  
DOI: 10.1039/x0xx00000x

## Results and discussion

### Synthesis of gold complexes:

As shown in Scheme 1, reaction of [AuCl(tht)] (tht = tetrahydrothiophene) with an equimolar amount of tris(4-methoxyphenyl)phosphine afforded the desired gold(I) chloride complex [AuCl{P(C<sub>6</sub>H<sub>4</sub>-4-OMe)<sub>3</sub>}] (**1**), from which the corresponding bromide (**2**) and iodide (**3**) complexes were prepared by metathetical reactions. Oxidation of **1** with chlorine (as PhCl<sub>2</sub>) gave the gold(III) complex [AuCl<sub>3</sub>{P(C<sub>6</sub>H<sub>4</sub>-4-OMe)<sub>3</sub>}] (**4**), while the cationic bis(phosphine) gold(I) complex [Au{P(C<sub>6</sub>H<sub>4</sub>-4-OMe)<sub>3</sub>}<sub>2</sub>]PF<sub>6</sub> (**5**) was prepared by treating **1** with one equivalent of phosphine in the presence of TlPF<sub>6</sub>.

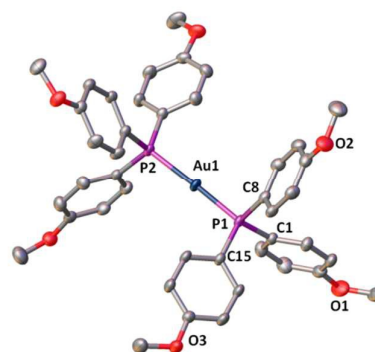


**Fig. 2** The molecular structure of [Au{P(C<sub>6</sub>H<sub>4</sub>-4-OMe)<sub>3</sub>}<sub>2</sub>]PF<sub>6</sub> (**5**). Ellipsoids show 50% probability levels. Hydrogen atoms and PF<sub>6</sub> counter ion have been omitted for clarity. Selected bond distances (Å) and angles (°): Au(1)-P(1) 2.3151(6), Au(1)-P(2) 2.3145(6), P(1)-Au(1)-P(2) 174.331(19).

**Scheme 1** Synthesis of neutral gold(I), gold(III) and cationic gold(I) complexes containing methoxy-substituted triaryl phosphine ligands.

Analogous to the preparation of **1-3**, [AuCl{P(C<sub>6</sub>H<sub>4</sub>-2,6-{OMe})<sub>2</sub>}] (**6**) was synthesized from the reaction of [AuCl(tht)] with tris(2,6-dimethylphenyl)phosphine, which was converted to the corresponding bromide (**7**) and iodide (**8**) complexes. The gold(III) complex [AuCl<sub>3</sub>{P(C<sub>6</sub>H<sub>4</sub>-2,6-{OMe})<sub>2</sub>}] (**9**) and cationic gold(I) complex [Au{P(C<sub>6</sub>H<sub>4</sub>-2,6-{OMe})<sub>2</sub>}<sub>2</sub>]PF<sub>6</sub> (**10**) were prepared following an analogous method for the synthesis of **4** and **5**, respectively. The preparation of complexes **1-3**,<sup>20</sup> **5** (as the perchlorate salt)<sup>21</sup> and **6**<sup>22</sup> have been reported previously; all other complexes are new. Complexes **1-10** were characterized by multinuclear NMR spectroscopy (<sup>1</sup>H and <sup>31</sup>P); complexes **4-10** were also characterized by single crystal X-ray diffraction.

In general agreement with the reported data (where available), the <sup>1</sup>H NMR spectra for complexes **1-10** each showed the expected aromatic multiplets between δ 6.5-7.5, together with a singlet resonance around δ 3-4 due to the methoxy protons in the correct integral ratio. Uniquely, in the case of the gold(III) complex [AuCl<sub>3</sub>{P(C<sub>6</sub>H<sub>4</sub>-2,6-{OMe})<sub>2</sub>}] (**9**), three singlet resonances were observed at δ 3.49, 3.62 and 3.94 arising from restricted rotation about the P-AuCl<sub>3</sub> bond. Similar restricted rotation about Au-P bonds in gold(III) complexes containing phosphine ligands with bulky *ortho*-substituents has been observed previously.<sup>23</sup> The <sup>31</sup>P NMR spectra for the gold complexes **1-4** and **6-9** each showed a singlet resonance in the expected region of *ca.* δ 35 and δ -25, respectively. The gold(III) complexes **5** and **10** similarly showed a singlet resonance, but are shifted downfield from their corresponding gold(I) counterparts by approximately 10 and 30 ppm, respectively. In addition, the expected septet at δ -144 due to PF<sub>6</sub> counter ion was also observed.

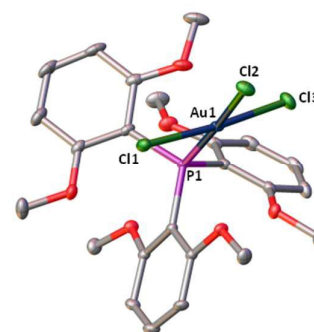


**Fig. 3** Molecular structure of [AuCl<sub>3</sub>{P(C<sub>6</sub>H<sub>3</sub>-2,6-{OMe})<sub>2</sub>}] (**9**). Ellipsoids show 30% probability levels. Hydrogen atoms have been omitted for clarity. Selected bond distances (Å) and angles (°): Au(1)-P(1) 2.3261(6), Au(1)-Cl(1) 2.2941(6), Au(1)-Cl(2) 2.3508(6), Au(1)-Cl(3) 2.2874(7), P(1)-Au(1)-Cl(2) 175.782(19).

The molecular structures of **4-10** were confirmed by X-ray diffraction, and the molecular structures of **5** and **9** are shown in Fig. 2 and 3, respectively. All other structures are shown in Fig. S11-S15 (see Supporting Information). In the structures of **5-8** and **10**, the gold(I) atom is coordinated by a phosphorus atom of the tertiary phosphine and a halide, or, in the case of **5** and **10**, by a second phosphorus atom. As expected, the geometry about the gold atom is approximately linear (173-179°), with Au-P bond lengths in the range 2.24-2.33 Å. The Au-X bond lengths in complexes **6-8** are typical for gold(I) halide complexes and increase in the order X = Cl (2.29 Å) < Br (2.42 Å) < I (2.56 Å). In the structures of **4** and **9**, the gold(III) atom is approximately square planar, the Au-Cl bond lengths *trans* chloride being *ca.* 2.27-2.29 Å, while those *trans* to phosphorus are significantly longer (*ca.* 2.35-2.37 Å) as a consequence of the higher *trans* influence of tertiary phosphines compared to chloride. In all cases, the metrical parameters in **4-10** are comparable to those observed for their

triphenylphosphine analogues  $[\text{AuX}(\text{PPh}_3)]$ ,<sup>24</sup>  $[\text{AuCl}_3(\text{PPh}_3)]$ <sup>25</sup> and  $[\text{Au}(\text{PPh}_3)_2]\text{PF}_6$ .<sup>26</sup> It has been reported that metal complexes are vulnerable to reduction in DMSO,<sup>27</sup> therefore we monitored the stability of complexes **1-10** in DMSO over a period of 72 h using <sup>31</sup>P NMR spectroscopy. The resulting spectral profiles are shown in Fig. S16-S25 in the Supporting Information. In most cases there was no observable shift in the characteristic peaks for the gold phosphine complexes over 72 h, suggesting the gold complexes are stable in DMSO. A change in the <sup>31</sup>P NMR spectrum of the gold(III) complex **4** in DMSO was observed after 1 h indicating decomposition. The stabilities of the synthesised gold complexes were also investigated under physiological-like conditions by monitoring the electronic absorption spectra of the complexes in a tris buffered saline solution (50 mM Tris, 150 mM NaCl, pH 7.2) over 72 h. As evident from the electronic spectra (Fig. S26), gold(I), gold(III), and ionic complexes under investigation displayed no change in the absorbance over time, indicating the complexes are stable under physiological-like condition over 72 h.

### *In vitro* anticancer activity

The cell growth inhibitory effects of the gold complexes **1-7**, **9** and **10** were evaluated towards a panel of five human tumor cell lines [ovarian (SKOV-3), fibrosarcoma (HT1080), glioblastoma (U87MG), prostate (PC-3), cervical (HeLa)] and normal human embryonic kidney (Hek-293T) cells using the MTT assay.<sup>28</sup> The gold iodide complex **8** proved to be too insoluble for testing and was not investigated further. The anticancer activities of the gold complexes, reported as IC<sub>50</sub> values, were compared to those obtained for cisplatin, which was used as a standard, and  $[\text{AuCl}(\text{PPh}_3)]$ , the parent unsubstituted gold complex. As shown in Table 1, nearly all of the newly synthesized complexes displayed remarkable antiproliferative effects against all the tested cancer cell lines. Notably, the presence of methoxy substituents on the phosphine ligand in the gold complexes significantly effects their anticancer activity and selectivity towards cancer cells. By comparison to  $[\text{AuCl}(\text{PPh}_3)]$ , (IC<sub>50</sub> 2.57-8.93 μM), the 4-methoxy-substituted complex **1** showed increased activity and selectivity (IC<sub>50</sub> 0.97-6.45 μM), and an even more substantial increase was observed for the 2,6-dimethoxy-substituted complex **6** (IC<sub>50</sub> 0.53-1.18 μM). Despite the different oxidation state, the neutral gold(III) complexes **4** and **9** displayed similar antiproliferative effects to their gold(I) counterparts **1** and **6**, respectively. Among all the complexes in the series, the cationic dimethoxy-substituted complex **10** displayed a potent and broad spectrum anticancer activity with IC<sub>50</sub> values in the submicromolar range (0.19-0.77 μM), significantly lower than the IC<sub>50</sub> values of cisplatin (0.63-8.22 μM). In particular, complex **10** showed approximately 30 fold higher cytotoxicity than cisplatin towards PC-3 and U87MG cells. The promising *in vitro* anticancer activities of the neutral gold(I) chloride complexes **1** and **6** and cationic complexes **5** and **10** prompted us to investigate their mechanism of cell death. We also investigated the effect of these complexes on normal kidney cells (HeK-293T) to determine the safety and selectivity against non-cancer cells. Interestingly, most of the synthesized complexes displayed potent cytotoxicity towards cancer cells in comparison to normal HeK-293T kidney cells. It was observed that the highly active cationic gold complex **10** showed 5-10 times higher selectivity towards various cancer cells.

**Table 1** IC<sub>50</sub> values (μM)\* of the gold complexes **1-7**, **9** and **10** towards various cancer cells and one normal cell line after 72 h exposure.

Complex	SKOV-3	HT1080	U87MG	PC-3	HeLa	Hek-293T
<b>1</b>	6.45±0.24	1.37±0.11	3.9±0.41	4.01±0.6	0.97±0.26	12.55±1.67
<b>2</b>	14.7±2.65	2.95±0.21	3.53±0.66	5.69±0.5	3.5±0.62	9.63±1.41
<b>3</b>	5.14±0.39	4.76±0.36	6.48±1.13	4.87±0.2	2.4±0.3	7.98±0.21
<b>4</b>	8.53±0.75	2.13±0.35	4.14±0.54	3.61±0.7	2.57±0.4	13.7±0.13
<b>5</b>	4.23±0.36	1.78±0.08	3.2±0.82	2.87±0.1	1.12±0.1	11.3±1.65
<b>6</b>	0.77±0.05	1.18±0.21	1.14±0.29	0.53±0.08	0.89±0.2	2.13±0.32
<b>7</b>	1.28±0.08	0.87±0.06	1.31±0.32	1.4±0.05	0.26±0.08	5.72±0.75
<b>9</b>	1.14±0.17	2.42±0.07	1.26±0.16	0.57±0.03	1.17±0.06	1.78±0.17
<b>10</b>	0.34±0.11	0.77±0.04	0.28±0.09	0.19±0.02	0.25±0.05	1.65±0.33
<b>AuCl(PPh<sub>3</sub>)</b>	8.93±1.21	4.66±0.63	5.57±0.28	4.53±0.74	2.57±0.16	1.98±0.23
<b>Cisplatin</b>	1.57±0.36	0.63±0.1	8.22±0.8	6.31±0.2	3.25±0.28	4.78±0.35

\*IC<sub>50</sub> values are the concentrations that cause 50% inhibition of cell growth. SKOV-3: ovarian; HT1080: fibrosarcoma; U87MG: glioblastoma; PC-3: prostate; HeLa: cervical; Hek-293T: normal human embryonic kidney cells. Data represent the mean values ± standard deviation of three independent experiments performed in triplicate.

### 3D Multicellular spheroid inhibition assay

3D Multicellular spheroids (MCSs) closely reflect the *in vivo* pathophysiological situation in tumor tissues with respect to phenotypic heterogeneity, nutrient and oxygen gradients and micro metastases with gene expression closer to the clinical expression profile.<sup>29-31</sup> For instance, tumor cells growing in 3D spheroids experience different adhesive, mechanical and topographical forces compared to cells growing in 2D monolayers. Moreover, the cell-cell, cell-ECM interactions of cells and permeability barrier in solid tumors could be imitated by establishment of tumor cell 3D spheroids. In a broad context, *in vitro* 3D tumor cell cultures could emerge as appropriate preclinical models to screen the cancer drug lead for solid tumors.<sup>32</sup> Therefore, to validate the cytotoxicity of the gold complexes in the *in vivo* tumor environment, 3D multicellular spheroids were generated by growing the cells in ultra-low attachment (ULA) plates for 2 days, which were then treated with IC<sub>50</sub> concentrations of the gold complexes, cisplatin, and auranofin. Fig. 4A depicts representative morphological changes of the MCSs after treatment with the gold complexes after 48 and 96 h. It is noted that treatment with the vehicle (DMSO) did not cause any growth inhibition and the volume of the spheroid increased over time during the experiment. In contrast, treatment with the gold complexes resulted in a reduction in surface area and volume of the

## ARTICLE

## Journal Name

spheroids and the effect is significant after 96 h. Treatment with the cationic complexes **5** and **10** lead to a significant reduction of spheroid volume and increased number of dead cells (propidium iodide stained) in comparison to the control (Fig. 4B), consistent with the results obtained from the 2D cell monolayer assays. These results indicate that the cytotoxic effects of the cationic compounds were equally potent in 3D spheroid cultures as they were in 2D cultures.

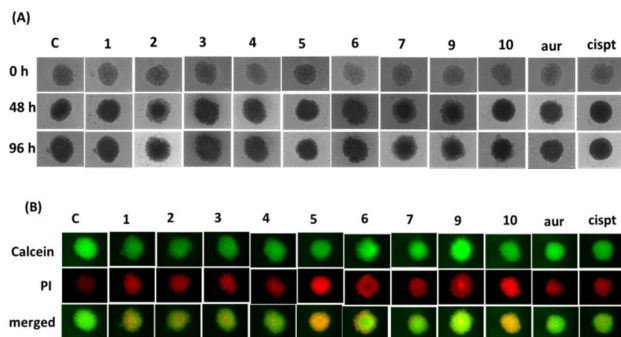


**Fig. 4** Antitumor potential of gold complexes in 3D HeLa multicellular spheroids. (A) HeLa cell spheroids were generated in 96-well ULA round-bottomed plates and were examined for the morphological changes immediately and after 48 and 96 h incubation with IC<sub>50</sub> concentrations of the gold complexes, auranofin, and cisplatin. (B) Representative images of Calcein AM/propidium iodide staining on HeLa MCSs after treatment with IC<sub>50</sub> concentrations of the metal complexes.

#### Effect of the gold complexes on cell migration

Migration of cancer cells plays an important role in the progression of tumors and metastasis.<sup>33</sup> Previous studies have demonstrated that gold complexes inhibit the migration of cancer cells.<sup>34-35</sup> To investigate whether the selected gold phosphine complexes **1**, **5**, **6** and **10** could inhibit *in vitro* cell migration, a wound healing assay was carried out using HeLa cervical cancer cells. The number of cells that migrated into the wound area was counted manually, and the calculated migration rate is reported in Fig. 5. The results, shown in Fig. 5A and 5B, indicate that, in comparison to the control, cell migration was significantly inhibited (30-40% inhibition) after 24 h treatment with the metal complexes, and the effect is even higher (40-60% inhibition) after 48 h.

#### Effect of the gold complexes on actin assembly

The polymerization of actin filaments is considered an essential step for the formation of cell membrane protrusions, which can help in cell migration as well as stress fibre assembly.<sup>36</sup> As shown in Fig. 5, the gold complexes inhibited the migration of HeLa cancer cells, so we next examined the effect the complexes had on actin polymerization. In this assay, the cytoskeleton of the HeLa cells treated with the gold complexes (**1**, **5**, **6** and **10**) was visualized using rhodamine phalloidin, a red fluorescent dye which specifically stains F-actin proteins. It was observed that treatment with the gold complexes causes a decrease in F-actin extensions at the periphery and inhibited the formation of stress fibre assemblies. The control cells displayed elongated stress fibres with broad lamellipodia whereas after treatment with the gold complexes, the staining was rather granulated and condensed (Fig. 6) and the tumor cells were

no longer capable of maintaining the characteristic broad lamellipodia. Collectively, these results indicate that gold complexes inhibit the migration of HeLa cancer cells through disruption of F-actin assembly and stress fibre formation.

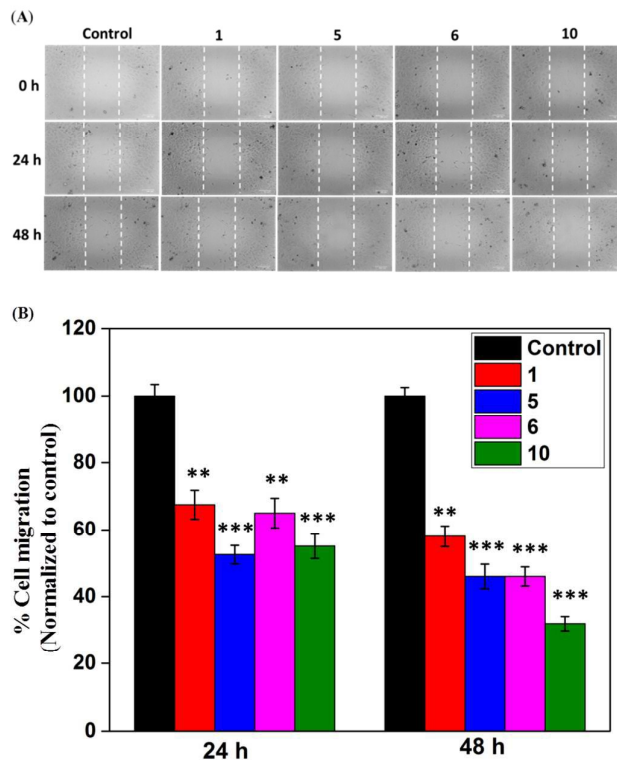


**Fig. 5** The effect of the gold complexes **1**, **5**, **6** and **10** on the migration of HeLa cells. (A) Wounds were created in the confluent monolayers and photos were taken at 0, 24 and 48 h after treatment with the gold complexes (4x magnification). (B) Graphical representation of the percentage of migration of HeLa cells after treatment with IC<sub>50</sub> concentrations of the gold complexes. Data are the mean of three independent experiments  $\pm$  the standard deviation (\*\*p < 0.01, \*\*\*p < 0.001).

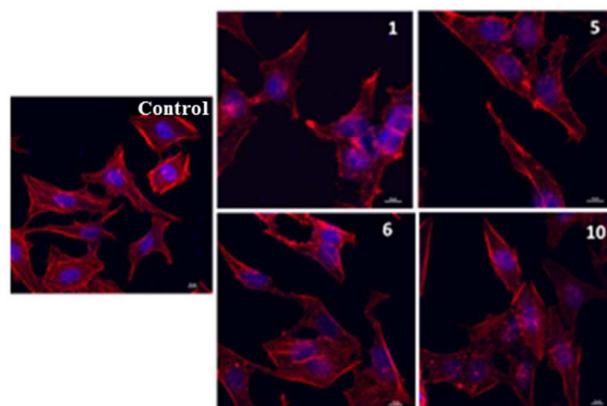


**Fig. 6** Disruption of F-actin assemblies due to the gold complexes **1**, **5**, **6**, and **10**. HeLa cells were treated with IC<sub>50</sub> concentrations of the gold complexes and stained with rhodamine-phalloidin (red fluorescent dye: actin filament) and Hoechst 33242 (nucleus: blue).

### TrxR inhibition

The thioredoxin (Trx) system consists of NADPH, thioredoxin reductase (TrxR), and Trx, and plays a central role in several cellular homeostasis processes, including the regulation of transcription factors and the removal of reactive oxygen species which overcomes oxidative stress.<sup>37</sup> Therefore, the inhibition of TrxR has recently emerged as an attractive strategy in cancer treatment since the overexpression of TrxR in various aggressive tumors is considered to be responsible for the development of drug resistance.<sup>38</sup> It has been shown that many of the reported gold(I) compounds exhibit antiproliferative activity through strong TrxR inhibition.<sup>39-40</sup> To investigate whether the newly synthesized gold complexes could inhibit TrxR in HeLa cells, the lipoate reduction assay was carried out.<sup>41</sup> In this assay, the ability of live HeLa cells to reduce the cell permeable cofactor (lipoate) was monitored colorimetrically over a period of 180 min after 6 h treatment with the gold complexes (**1**, **5**, **6** and **10**). Auranofin was used as a positive control in this experiment. As shown in Fig. 7, treatment with the neutral gold complexes **1** and **6** lead to strong inhibition of TrxR (70-80%) in HeLa cells in comparison to auranofin. Moreover, a significant inhibition of TrxR (50-60%) was observed for the cationic complexes **5** and **10** relative to the vehicle treated control cells. The higher TrxR inhibition of the neutral gold(I) complexes may be due to participation in ligand exchange reactions with the selenocysteine residue of TrxR. Overall, these results indicate the newly synthesized gold complexes are comparable to auranofin in their ability to inhibit TrxR in HeLa cells.

### Reactive oxygen species (ROS)

It is well-known that TrxR enzyme inhibition causes an increase in hydrogen peroxide and reactive oxygen species levels which leads to an imbalance in cell redox conditions, thus resulting in mitochondrial membrane permeabilization and cell apoptosis.<sup>42</sup> To determine if the TrxR inhibitory properties of the gold complexes would lead to increased ROS levels in HeLa cells, we carried out a ROS assay using 6-carboxy-2',7'-dichlorodihydrofluorescein diacetate (Carboxy-DCFDA), a non-fluorescent dye which, on hydrolysis by ROS, produces green fluorescent DCF. The intensity of the DCF fluorescence directly correlates with the intracellular ROS levels and is measured by flow cytometry. As shown in Fig. 8, a 2-4 fold increase in DCF fluorescence was observed due to H<sub>2</sub>DCF oxidation after treatment with the complexes **1**, **5**, **6** and **10** in comparison to the control cells, indicating the gold complex treatment leads to an increase in ROS levels. Based on these results, we propose that the antiproliferative activity of the gold complexes was due to TrxR based ROS mediation.

### Cell cycle distribution

To investigate the influence of the gold complexes on the cell cycle distribution of HeLa cells, propidium iodide staining was carried out. The cells were treated with complexes **1**, **5**, **6** and **10** and after 48 h analysed by flow cytometry (Fig. 9). The results from the histograms indicate that the gold complexes induce apoptosis in HeLa cells with a profound increase of sub G1 cell population. Quantitative analysis revealed that, compared to the control cells (2.6%), the percentage of sub G1 phase cells increased significantly to 9.6, 16.3, 11.1 and 18.5% after treatment with complexes **1**, **5**, **6** and **10**, respectively (Fig. 9B). Simultaneously, a significant decrease in the cell

population in the G0/G1 phase was observed after treatment with the complexes. Moreover, complex treatment leads to an increase in the S phase population without altering the G2/M phase. These results indicate the metal complexes inhibit the cell cycle progression in the S phase and also induce apoptosis through sub G1 arrest.

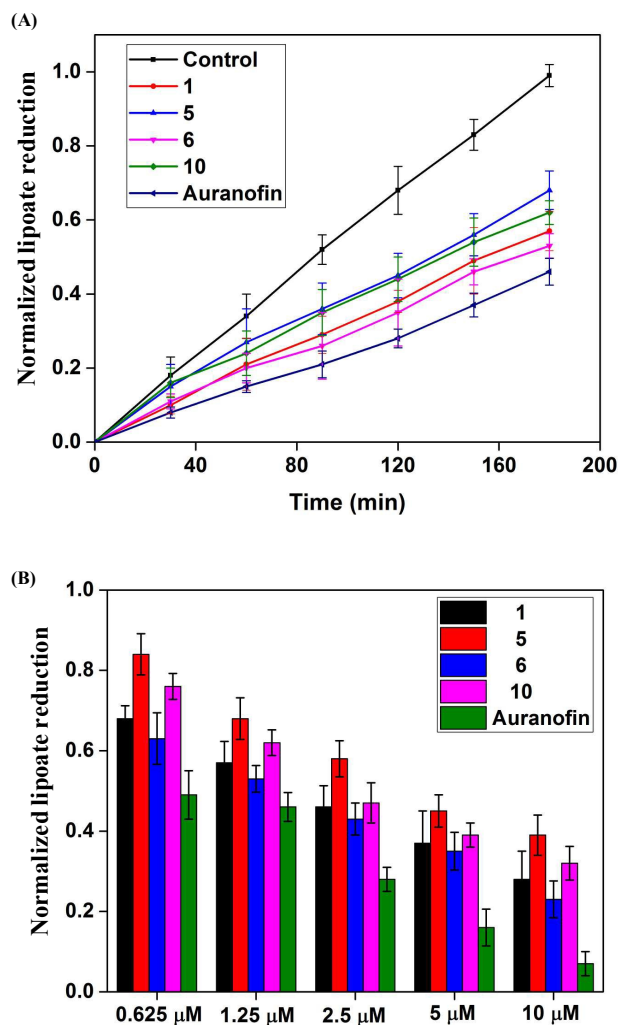


**Fig. 7** (A) TrxR inhibitory activity of the gold complexes **1**, **5**, **6** and **10** in HeLa cells after treatment with 1.25 μM concentration over a period of 180 min. (B) Concentration-dependent inhibition of TrxR activity in HeLa cells treated with 0.625–10.0 μM gold complexes for 6 h and monitoring the lipoate reduction colorimetrically after 180 min incubation.

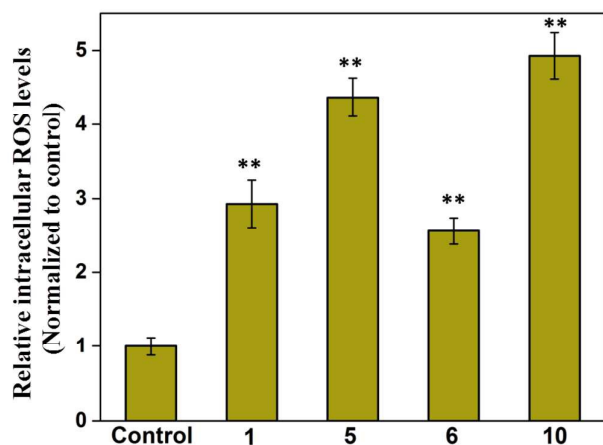


**Fig. 8** Effect of the gold complexes **1**, **5**, **6** and **10** on the production of ROS in HeLa cells. ROS levels were determined by monitoring the fluorescence of DCF via flow cytometric analysis in live HeLa cells treated with the complexes. The fold increase in ROS was quantified using BD Accuri C6 software. Error bars represent one standard deviation. Data are the mean of three independent experiments  $\pm$  the standard deviation (\* $p < 0.05$ , \*\* $p < 0.01$ ).

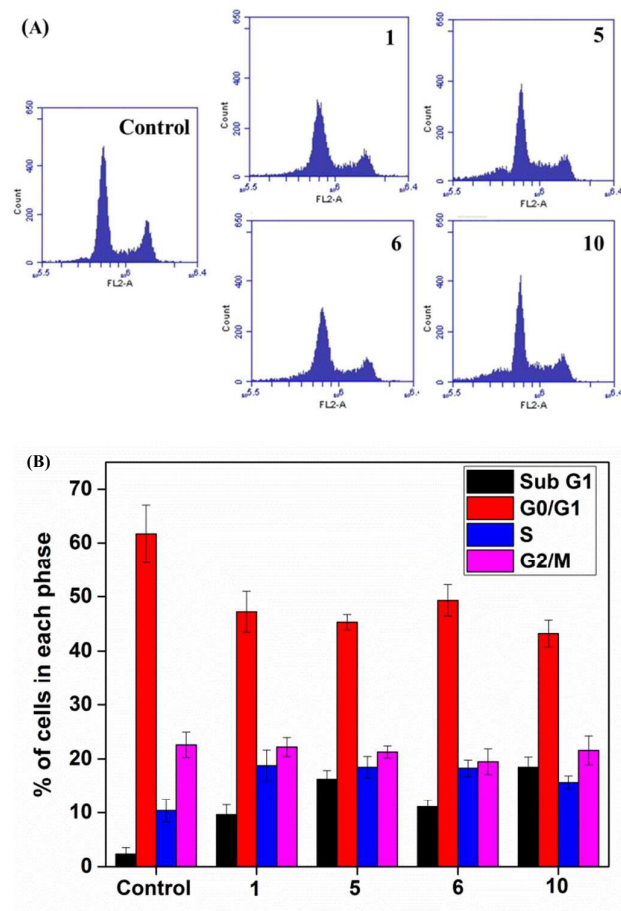


**Fig. 9** (A) Effect of gold complexes **1**, **5**, **6** and **10** on the cell cycle distribution of HeLa cells after treatment with  $IC_{50}$  concentrations

for 48 h. Propidium iodide stained cells were analysed by flow cytometry. Data from 10,000 cells were collected for each data file. Histograms are representatives of three independent experiments. (B) The percentage of cells in each phase (G0/G1, S, and G2/M) was quantified using BD Accuri C6 software.

#### Caspase-3 activity assay

Previous reports have suggested that gold(I) complexes can induce apoptosis in cancer cells through the activation of caspases.<sup>43-44</sup> Among the caspases, caspase-3 is the main downstream effector caspases, and the activation of this enzyme leads to the cleavage of a variety of critical cellular proteins.<sup>45</sup> Therefore, we investigated the ability of the gold complexes **1**, **5**, **6** and **10** to activate caspase-3 in HeLa cells after 24 h treatment with  $IC_{50}$  concentrations. As shown in Fig. 10, treatment with the gold complexes markedly stimulated caspase-3 activity in comparison to the control. The increment of caspase-3 concentration was significant for all complexes relative to the control with a 2-3 fold increase in caspase-3 activity. Taken together, these results indicate that HeLa cells treated with the gold complexes showed several hallmarks of apoptotic cell death, including strong induction of caspase-3 activity.

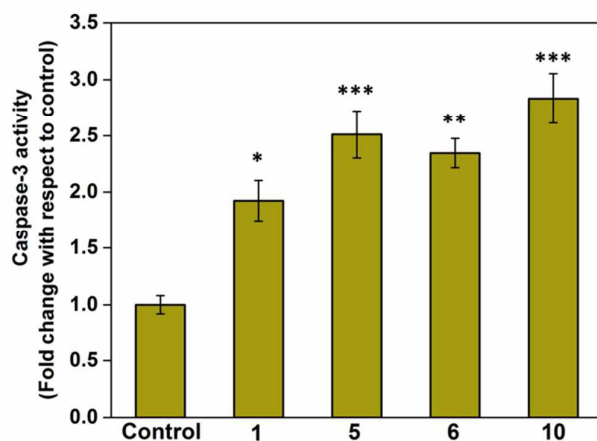


**Fig. 10** Caspase-3 activity in HeLa cells after treatment with complexes **1**, **5**, **6**, and **10** for 24 h. Caspase-3 activation was determined by mixing the cell lysates with DEVD-pNA (N-acetyl-Asp-Glu-Val-Asp p-nitroanilide) and monitoring the colorimetric substrate hydrolysis at 405 nm using an absorbance plate reader. The values are shown as a fold-increase compared to the control. Data are the mean of three independent experiments  $\pm$  the standard deviation (\* $p < 0.05$ , \*\* $p < 0.01$ , \*\*\* $p < 0.001$ ).

#### Hoechst staining

It was considered of interest to examine the effect of the gold complexes on morphological changes, such as DNA fragmentation associated with caspase-3 and increased ROS, which are known to cause apoptosis.<sup>46</sup> HeLa cells treated with  $IC_{50}$  concentrations of the gold complexes **1**, **5**, **6** and **10** for 48 h were stained with the nuclear staining dye Hoechst 33342. The results, shown in Fig. 11, indicated that untreated control cells showed no obvious morphological changes (all the cells exhibited uniform rounded cell morphology), whereas treatment with the gold complexes lead to

fragmentation of nuclei (indicated by red arrows), which is a hallmark of apoptosis. As expected, the cationic complexes **5** and **10** were potent in inducing nuclear fragmentation in HeLa cells.

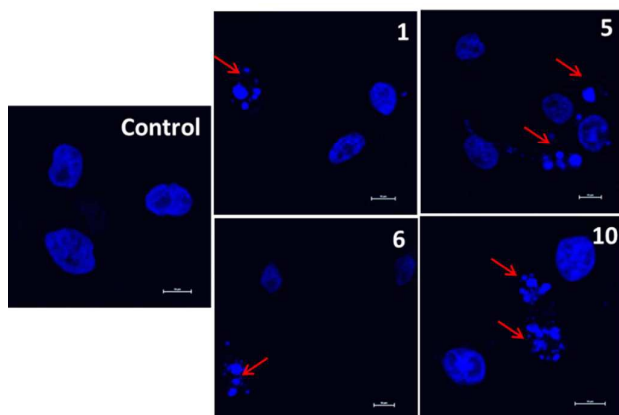


**Fig. 11** Nuclear morphological changes in HeLa cells after treatment with  $IC_{50}$  concentrations of the gold complexes **1**, **5**, **6** and **10** for 48 h (red arrows indicate fragmented nuclei-apoptotic cells).

#### Annexin V-FITC/propidium iodide dual staining assay

Since the metal complexes induce apoptosis in HeLa cells through sub G1 cell cycle arrest and caspase-3 stimulation, the Annexin V-FITC/propidium iodide double staining assay was carried out to quantify the gold complex-induced apoptosis. As shown in Fig. 12, the populations of early apoptotic (LL) and late apoptotic (LR) cells were dramatically increased to 22.6–42.3% after treatment with the gold complexes in comparison to the vehicle treated cells (10.9%). The cationic complexes **5** and **10** were potent in inducing apoptosis, with more than 40% of the cells being apoptotic whereas the neutral gold complexes **1** and **6** displayed approximately 25% of the apoptotic cells. These results further confirm the apoptosis-inducing ability of the gold complexes in HeLa cells.

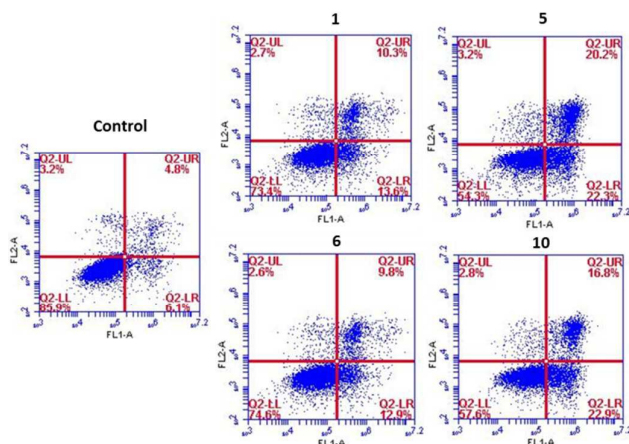


**Fig. 12** Flow cytometric analysis of the apoptotic and necrotic cells induced by the gold complexes **1**, **5**, **6** and **10**. HeLa cells were stained with Annexin V-FITC and PI after 48 hours of incubation with the  $IC_{50}$  concentrations of the metal complexes (LL: live; LR: early apoptotic; UR: late apoptotic; UL: necrotic).

#### Conclusions

In conclusion, we have synthesized a series of gold complexes containing methoxy-substituted aryl phosphine ligands and investigated their anticancer properties towards a panel of five different human tumor cell lines. Most of the synthesized complexes displayed promising *in vitro* anticancer activities with  $IC_{50}$  values in the range of low micromolar and even nanomolar concentrations on various cancer cell lines. The structure activity relationships of the gold complexes reveal that methoxy substituents on the phosphine ligand are crucial for the enhanced anticancer activity and selectivity towards cancer cells. Among the series, the lipophilic cationic complexes **5** and **10** displayed potent cytotoxicity towards all the tested cell lines with  $IC_{50}$  values in the range of 0.19–0.77  $\mu$ M. In contrast, the neutral hydrophilic gold(III) complexes **4** and **9**, and their gold(I) counterparts **1** and **6**, displayed similar antiproliferative effects with moderate cytotoxicity. It was also observed that there was no significant correlation between the halide bound to gold (Cl, Br, I) and their cytotoxicity. The more physiologically relevant 3D tumor spheroid assay demonstrates the superior potency of these cationic complexes. It is also evident that the observed significant cytotoxicity of the gold complexes was through TrxR inhibition, increased ROS and apoptosis induction with sub G1 cell cycle arrest and caspase-3 activation. Taken together, these findings clearly demonstrate the potential of the gold(I) complexes in anticancer drug development.

#### Experimental

##### Chemistry

Tris(4-methoxyphenyl)phosphine and tris(2,6-dimethoxyphenyl)phosphine were purchased from Sigma.  $[PhICl_2]$ ,<sup>47</sup>  $[AuCl(tht)]$ <sup>48</sup> and  $[AuCl(PPh_3)]$ <sup>49</sup> were prepared following literature methods.  $[AuX\{P(C_6H_4-4-OMe)_3\}]$  (X = Cl, Br, I) were prepared by a modified literature method, the details of which are given below.  $^1H$  (300 MHz) and  $^{31}P$  (121 MHz) NMR spectra were measured as  $CDCl_3$  solutions on a Bruker Avance 300 spectrometer at room temperature. Chemical shifts are referenced to residual solvent signals ( $^1H$ ) or external 85%  $H_3PO_4$  ( $^{31}P$ ) and coupling constant ( $J$ ) are given in Hz. Mass spectra were acquired on a Bruker Autoflex Speed (MALDI) or Perkin Elmer Axion 2 TOF (ESI) spectrometer. In general, the mass spectra for the gold(I) halide complexes failed to show peaks assignable to the  $[M]^+$  or  $[M-halide]^+$  fragments, but intense peaks due to the  $[AuL_2]^+$  ion; similar behaviour has been reported previously.<sup>50</sup>

##### X-ray crystallography

Crystals of complexes **4–10** suitable for single-crystal X-ray diffraction were obtained from dichloromethane/hexane. Using a drop of inert oil (Nujol), crystals were mounted on a nylon loop and transferred into a stream of cold nitrogen. The reflections were collected on a D8 Bruker diffractometer equipped with an APEX-II area detector using graphite-monochromated Mo K $\alpha$  radiation ( $\lambda = 0.71073 \text{ \AA}$ ) from a 1  $\mu$ S microsource. The computer programs SMART<sup>51</sup> and SAINT<sup>52</sup> were used for data collection in  $\phi$ - and  $\omega$ -scan modes and data processing, respectively, and absorption corrections using SADABS.<sup>53</sup> The structures were solved using direct methods and refined with full-matrix least-squares methods

on  $F^2$  using the SHELX-TL package.<sup>54-55</sup> The CCDC numbers for complexes **4-10** are 1811850-1811856.

#### Preparation of [AuCl{P(C<sub>6</sub>H<sub>4</sub>-4-OMe)<sub>3</sub>}] (1)

To a solution of [AuCl(tht)] (0.91 g, 2.83 mmol) in CH<sub>2</sub>Cl<sub>2</sub> (30 mL), cooled to 0°C, was added P(C<sub>6</sub>H<sub>4</sub>-4-OMe)<sub>3</sub> (1.00 g, 2.83 mmol). The clear colorless solution was stirred for 30 min, filtered through Celite and MeOH added to the filtrate. The volume of the solution was reduced *in vacuo*, precipitating a white solid, which was filtered off, washed with MeOH and dried *in vacuo*. <sup>1</sup>H NMR: δ 7.41-7.50 (m, 6H), 6.95-7.00 (m, 6H), 3.87 (s, 9H). <sup>31</sup>P NMR: δ 29.2 (s). MALDI-MS (*m/z*): 901.28 [AuL<sub>2</sub>]<sup>+</sup>, 1133.26 [Au<sub>2</sub>L<sub>2</sub>Cl]<sup>+</sup>.

#### Preparation of [AuBr{P(C<sub>6</sub>H<sub>4</sub>-4-OMe)<sub>3</sub>}] (2)

To a solution of [AuCl{P(C<sub>6</sub>H<sub>4</sub>-4-OMe)<sub>3</sub>}] (150 mg, 0.26 mmol) in CH<sub>2</sub>Cl<sub>2</sub> (10 mL) was added a solution of LiBr (35 mg, 0.40 mmol) in MeOH (5 mL). After stirring the solution for 15 min, the solvent was removed *in vacuo* and the residue was dissolved in CH<sub>2</sub>Cl<sub>2</sub>. Filtration through Celite gave a clear solution, to which MeOH was added. The volume of the solution was reduced *in vacuo*, precipitating a white solid which was filtered off, washed with MeOH and dried *in vacuo* (118 mg, 73%). <sup>1</sup>H NMR: δ 7.42-7.49 (m, 6H), 6.96-6.99 (m, 6H), 3.86 (s, 9H). <sup>31</sup>P NMR: δ 31.6 (s). MALDI-MS (*m/z*): 901.34 [AuL<sub>2</sub>]<sup>+</sup>, 1177.28 [Au<sub>2</sub>L<sub>2</sub>Br]<sup>+</sup>.

#### Preparation of [AuI{P(C<sub>6</sub>H<sub>4</sub>-4-OMe)<sub>3</sub>}] (3)

Compound **3** was prepared analogously to the bromo complex above from [AuCl{P(C<sub>6</sub>H<sub>4</sub>-4-OMe)<sub>3</sub>}] (150 mg, 0.26 mmol) and NaI (60 mg, 0.40 mmol) to give the product as a white solid (166 mg, 96%). <sup>1</sup>H NMR: δ 7.43-7.50 (m, 6H), 6.97-7.00 (m, 6H), 3.86 (s, 9H). <sup>31</sup>P NMR: δ 35.9 (s). MALDI-MS (*m/z*): 901.32 [AuL<sub>2</sub>]<sup>+</sup>, 1225.23 [Au<sub>2</sub>L<sub>2</sub>I]<sup>+</sup>.

#### Preparation of [AuCl<sub>3</sub>{P(C<sub>6</sub>H<sub>4</sub>-4-OMe)<sub>3</sub>}] (4)

To a solution of [AuCl{P(C<sub>6</sub>H<sub>4</sub>-4-OMe)<sub>3</sub>}] (150 mg, 0.26 mmol) in CH<sub>2</sub>Cl<sub>2</sub> (10 mL) was added a solution of PhICl<sub>2</sub> (74 mg, 0.27 mmol) in CH<sub>2</sub>Cl<sub>2</sub> (10 mL). The colorless solution turned yellow and was left to stir for 10 min. The solvent was removed *in vacuo* and the residue dissolved in CH<sub>2</sub>Cl<sub>2</sub>. After filtration through Celite, hexane was added and the volume of the solution was reduced *in vacuo*, precipitating a bright yellow solid, which was filtered off, washed with hexane and dried *in vacuo* (162 mg, 96%). <sup>1</sup>H NMR: δ 7.60-7.67 (m, 6H), 7.07-7.03 (m, 6H), 3.92 (s, 9H). <sup>31</sup>P NMR: δ 41.3 (s).

#### Preparation of [Au{P(C<sub>6</sub>H<sub>4</sub>-4-OMe)<sub>3</sub>}]<sub>2</sub>PF<sub>6</sub> (5)

To a solution of [AuCl{P(C<sub>6</sub>H<sub>4</sub>-4-OMe)<sub>3</sub>}] (151 mg, 0.26 mmol) in CH<sub>2</sub>Cl<sub>2</sub> (10 mL) was added P(C<sub>6</sub>H<sub>4</sub>-4-OMe)<sub>3</sub> (91 mg, 0.26 mmol) and TlPF<sub>6</sub> (95 mg, 0.27 mmol). The suspension was stirred in the dark for 1 h then filtered through Celite. Hexane was added to the filtrate and the volume of the solution was reduced *in vacuo*. The white solid that precipitated was filtered off, washed with hexane and dried *in vacuo* (265 mg, 98%). <sup>1</sup>H NMR: δ 7.39-7.46 (m, 12H), 7.09-7.12 (m, 12H), 3.90 (s, 18H). <sup>31</sup>P NMR: δ 41.9 (s), -144.3 (sept, *J*<sub>PF</sub> = 712 Hz). MALDI-MS (*m/z*): 901.33 [M-PF<sub>6</sub>]<sup>+</sup>.

#### Preparation of [AuCl{P(C<sub>6</sub>H<sub>3</sub>-2,6-OMe)<sub>2</sub>}] (6)

To a solution of [AuCl(tht)] (0.716 g, 2.23 mmol) in CH<sub>2</sub>Cl<sub>2</sub> (30 mL), cooled to -20°C, was added P(C<sub>6</sub>H<sub>3</sub>-2,6-OMe)<sub>2</sub> (1.000 g, 2.24 mmol). The clear, colorless solution was stirred for 15 min, during which time a white precipitate formed. After warming to room temperature, the solid dissolved and the solution was filtered through Celite. MeOH was added to the filtrate, and the volume of the solution was reduced *in vacuo*. The white precipitate was filtered off, washed with MeOH and dried *in vacuo* (1.45 g, 96%). <sup>1</sup>H NMR: δ 7.29 (t, *J* = 8.3 Hz, 3H), 6.50 (dd, *J*<sub>HH</sub> = 8.3 Hz, *J*<sub>PH</sub> = 4.5 Hz, 6H), 3.56 (s, 18H). <sup>31</sup>P NMR: δ -32.5 (s). MALDI-MS (*m/z*): 1081.38 [AuL<sub>2</sub>]<sup>+</sup>, 1313.34 [Au<sub>2</sub>L<sub>2</sub>Cl]<sup>+</sup>.

#### Preparation of [AuBr{P(C<sub>6</sub>H<sub>3</sub>-2,6-OMe)<sub>2</sub>}] (7)

To a solution of [AuCl{P(C<sub>6</sub>H<sub>3</sub>-2,6-OMe)<sub>2</sub>}] (150 mg, 0.22 mmol) in CH<sub>2</sub>Cl<sub>2</sub> (30 mL) was added a solution of NaBr (35 mg, 0.34 mmol) in MeOH (15 mL). After stirring the solution for 10 min, the solvent was removed *in vacuo* and the residue was dissolved in CH<sub>2</sub>Cl<sub>2</sub>. The mixture was filtered through Celite and MeOH was added to the filtrate. The volume of the solution was reduced *in vacuo*, precipitating a white solid which was filtered off, washed with MeOH and dried *in vacuo* (153 mg, 96%). <sup>1</sup>H NMR: δ 7.29 (t, *J* = 8.3 Hz, 3H), 6.51 (dd, *J*<sub>HH</sub> = 8.3 Hz, *J*<sub>PH</sub> = 4.5 Hz, 6H), 3.56 (s, 18H). <sup>31</sup>P NMR: δ -28.5 (s). MALDI-MS (*m/z*): 636.06 [M-Br]<sup>+</sup>, 1081.28 [AuL<sub>2</sub>]<sup>+</sup>, 1357.21 [Au<sub>2</sub>L<sub>2</sub>Br]<sup>+</sup>.

#### Preparation of [Au{P(C<sub>6</sub>H<sub>3</sub>-2,6-OMe)<sub>2</sub>}] (8)

Compound **8** was prepared analogously to the bromo complex above from [AuCl{P(C<sub>6</sub>H<sub>3</sub>-2,6-OMe)<sub>2</sub>}] (150 mg, 0.22 mmol) and NaI (50 mg, 0.33 mmol) to give the product as a white solid (165 mg, 97%). <sup>1</sup>H NMR: δ 7.30 (t, *J* = 8.2 Hz, 1H), 6.51 (dd, *J*<sub>HH</sub> = 8.3 Hz, *J*<sub>PH</sub> = 4.5 Hz, 2H), 3.56 (s, 6H). <sup>31</sup>P NMR: δ -20.9 (s). MALDI-MS (*m/z*): 1081.34 [AuL<sub>2</sub>]<sup>+</sup>.

#### Preparation of [AuCl<sub>3</sub>{P(C<sub>6</sub>H<sub>3</sub>-2,6-OMe)<sub>2</sub>}] (9)

To a solution of [AuCl{P(C<sub>6</sub>H<sub>3</sub>-2,6-OMe)<sub>2</sub>}] (400 mg, 0.6 mmol) in CH<sub>2</sub>Cl<sub>2</sub> (20 mL), cooled to -78°C, was added a solution of PhICl<sub>2</sub> (165 mg, 0.6 mmol) in CH<sub>2</sub>Cl<sub>2</sub> (10 mL). The colorless solution turned yellow, the cold bath was removed, and the solution was left to stir for 10 min. The solution was filtered through Celite and hexane was added to the filtrate. The volume of the solution was reduced *in vacuo*, precipitating an orange solid, which was filtered off, washed with hexane and dried *in vacuo* (430 mg, 97%). <sup>1</sup>H NMR: δ 7.39 (t, *J* = 8.5 Hz, 3H), 6.4-6.6 (m, 6H), 3.94 (s, 6H), 3.62 (s, 6H), 3.49 (s, 6H). <sup>31</sup>P NMR: δ 2.5 (s). ESI-MS (*m/z*): 709.0577 [M-Cl]<sup>+</sup>. Calcd for C<sub>24</sub>H<sub>27</sub>AuCl<sub>2</sub>O<sub>6</sub>P: 709.0588

#### Preparation of [Au{P(C<sub>6</sub>H<sub>3</sub>-2,6-OMe)<sub>2</sub>}]<sub>2</sub>PF<sub>6</sub> (10)

To a solution of [AuCl{P(C<sub>6</sub>H<sub>3</sub>-2,6-OMe)<sub>2</sub>}] (120 mg, 0.18 mmol) in CH<sub>2</sub>Cl<sub>2</sub> (20 mL) was added P(C<sub>6</sub>H<sub>3</sub>-2,6-OMe)<sub>2</sub> (79 mg, 0.18 mmol) and TlPF<sub>6</sub> (65 mg, 0.19 mmol). The suspension was stirred in the dark for 1 h then filtered through Celite. Hexane was added to the filtrate and the volume of the solution was reduced *in vacuo*. The white solid that precipitated was filtered off, washed with hexane and dried *in vacuo* (216 mg, 99%). <sup>1</sup>H NMR: δ 7.33 (t, *J* = 8.3 Hz, 6H), 6.51 (dt, *J*<sub>HH</sub> = 8.3 Hz, *J*<sub>PH</sub> = 2.2 Hz, 12H), 3.28 (s, 36H). <sup>31</sup>P NMR: δ -22.0 (s), -144.3 (sept, *J*<sub>PF</sub> = 712 Hz). MALDI-MS (*m/z*): 1081.32 [M-PF<sub>6</sub>]<sup>+</sup>.

### Cell culture

Ovarian (SKOV-3), prostate (PC-3), fibrosarcoma (HT1080), glioblastoma (U87MG) and normal human embryonic kidney (HeK-293T) cells were obtained from the American Type Culture Collection (Rockville, MD, USA). Cervical (HeLa) cancer cells were generously provided by Professor Joseph Trapani (Peter MacCullum Cancer Centre, Melbourne). PC-3 and HeLa cells were grown in Roswell Park Memorial Institute (RPMI-1640, GIBCO) media whereas SKOV-3, HT1080, U87MG and Hek-293T were cultured in Dulbecco's Modified Eagle's Medium (DMEM, GIBCO) media; in both cases the media were supplemented with 1% penicillin-streptomycin and 10% FBS (Foetal Bovine Serum). All cells were maintained in an incubator humidified atmosphere containing 95% air and 5% CO<sub>2</sub> at 37 °C. 0.05% Trypsin-EDTA (ethylenediaminetetraacetic acid) was used for harvesting cells for subculture. For all the assays, stock solutions of the gold complexes were prepared in DMSO (10 mM) and the final treatment concentrations (0.01-100 μM) were made in complete growth medium.

### MTT assay

The MTT {3-(4,5-dimethylthiazol-2-yl)-2,5-diphenyltetrazolium bromide} assay is based on the reduction of a yellow coloured MTT solution to purple formazan crystals by the active mitochondria of viable cells. Thus, the amount of produced formazan crystals is proportional to the number of viable cells. In this assay, SKOV-3, PC-3, HT1080, U87MG, HeLa cancer cells and normal HeK-293T cells were seeded in a 96 well plate at a density depending on their doubling times, and cells were incubated overnight at 37 °C. After incubation, the cells were exposed to different concentrations (100, 10, 1, 0.1 and 0.01 μM) of the metal complexes **1-8** and **10** for 72 h. 1% DMSO in complete medium was used as a vehicle control. At the end of the incubation, the medium containing metal complexes was removed, and 100 μL of MTT solution (0.5 mg/mL in serum-free medium) was added to each well and further incubated for 4 h in the dark at 37 °C. The excess unreacted MTT was removed and the formazan crystals were dissolved in 100 μL of DMSO. The absorbances of the solutions were recorded at 570 nm using a micro plate reader (SpectraMax, Molecular Device). Cell viability was calculated as the percentage ratio of sample absorbance to the vehicle treated control absorbance. The IC<sub>50</sub> values were calculated using Probit software [29]. The results are presented as means of three independent experiments.

### Spheroid inhibition assay

HeLa cells (5000 cells/well) were seeded in 96 well ULA (ultra-low attachment) round-bottom plates and allowed to grow spheroids for 2 days. The spheroids of approximately 100 μm were treated with IC<sub>50</sub> concentrations of the gold complexes or cisplatin for a period of 96 h. The culture media from the wells were refreshed every two days without altering the drug concentration. The growth and surface area of the spheroids were monitored using phase contrast microscopy after 48 and 96 h treatment. To visualize the live/dead cells after 72 h treatment with the complexes, 3D spheroids were incubated with Calcein AM (2 μM) and propidium iodide (4 μM) for 30 minutes and imaged directly using an inverted fluorescence microscope. Live cells were distinguished by the presence of ubiquitous intracellular esterase activity, as determined by the enzymatic conversion of the virtually non-fluorescent cell-permeant calcein AM to the intensely green fluorescent calcein (ex

495 nm, em 515 nm). Propidium iodide would enter cells with damaged membranes and undergo a 40-fold enhancement of fluorescence after binding with nucleic acids, producing a bright red fluorescence in dead cells (ex 535 nm, em 617 nm).

### Wound healing assay

HeLa cells (2×10<sup>5</sup>/mL) were seeded in a 6 well plate in 2 mL complete medium and incubated overnight. Wounds were created across the well using a 200 μL pipette tip then washed with PBS (phosphate buffered saline) to remove the cell debris. The cells were incubated for a further 48 h either with or without the gold phosphine complexes (IC<sub>50</sub> concentrations) in complete growth medium. The cells were observed under an inverted microscope at 4× magnification immediately (0 h) and after 24 and 48 h treatment. The number of cells migrated into the wound area were counted manually. The data reported in Fig. 5B are the mean ± standard deviation from three independent experiments.

### Effect on F-actin

HeLa cells (2×10<sup>5</sup>/well) were seeded on cover slips in a 6 well plate and allowed to adhere overnight. After 24 h treatment with the gold complexes, the cells were washed with PBS (phosphate buffered saline) and fixed with 4% paraformaldehyde. After fixation, the cells were permeabilized with 0.01% Triton-X100 and incubated with rhodamine phalloidin (Thermo Fisher) for 1 h at room temperature. The excess dye was removed by washing with PBS and the cells were further incubated with Hoechst 33242 (2 μg/mL) for 10 min at room temperature to counterstain the nucleus. The coverslips were then mounted with ProLong Gold anti-fade reagent (Molecular probes), and the cells were observed under a confocal microscope (Nikon). Images were captured using 20× objective lens.

### TrxR inhibition assay (Lipoate reduction assay)

This assay involves addition of DTNB [5,5'-dithiobis(2-nitrobenzoic acid)] to the cells followed by lipoate (cell permeable cofactor) addition and measuring the formation of newly reduced thiol. HeLa cells (10000 cells/well) in a 96 well plate were seeded and allowed to grow overnight. The cells were incubated with different concentrations of the gold complexes (0.625, 1.25, 2.5, 5 and 10 μM) in complete growth medium for 6 h. Then, the medium containing the gold complexes was removed from the each well and replaced with 100 μL of HBSS (Hanks balanced salt solution) containing 20 mM lipoate and 1 mM DTNB. The plates were monitored immediately and every 30 min for a change in absorbance due to the reduction of DTNB at 405 nm over a period of 180 min using a micro plate reader (SpectraMax, Molecular Device).

### Reactive Oxygen Species

HeLa cells (2×10<sup>5</sup>/well) in a 6 well plate were cultivated under standard conditions and were incubated with the gold complexes for 48 h. After incubation, cells were harvested and resuspended in 1 mL of PBS buffer containing 10 μM CM-DCFDA (6-carboxy-2',7'-dichlorodihydrofluorescein diacetate) at room temperature in the dark for 15 min. The excess dye was removed by washing with PBS, and the cells were immediately analyzed for green fluorescence using a BD Accuri C6 flow cytometer.

### Cell cycle

## ARTICLE

## Journal Name

HeLa cells were seeded into a 6 well plate at a density of  $2 \times 10^5$  cells per well and allowed to adhere overnight. The cells were incubated with  $IC_{50}$  concentrations of the gold complexes in complete culture medium for 48 h. After incubation, the cells were harvested using 0.25% trypsin-EDTA, washed with cold PBS and fixed with 70% cold ethanol. The ethanol-fixed cells were further washed with PBS and stained with propidium iodide staining buffer. Then, 10000 cells from each sample were analysed for propidium iodide fluorescence using a BD Accuri C6 flow cytometer.

**Hoechst Staining**

The nuclear morphological changes induced by the gold complexes was analysed using Hoechst 33242. In this assay, HeLa cells ( $2 \times 10^5$ ) grown on cover slips were treated with  $IC_{50}$  concentrations of the gold complexes for 48 h. The cells were washed with PBS, fixed with 4% paraformaldehyde and stained with Hoechst 33242 (2  $\mu\text{g}/\text{mL}$ ) for 15 min at room temperature. The excess dye was removed by washing with PBS and the cells were observed under a confocal microscope (Nikon).

**Caspase-3 assay**

Caspase-3 activation was determined using a colorimetric Caspase-3 Assay Kit (Thermo Fischer, khz0022). HeLa Cells ( $2 \times 10^5$  cells/well) incubated with  $IC_{50}$  concentration of the complexes for 24 h were harvested with 0.05% trypsin-EDTA and washed with PBS. The pellets were then resuspended in lysis buffer (50  $\mu\text{L}$ ) for 20 min. Cell lysates were centrifuged at 15000 rpm for 10 min at 4  $^{\circ}\text{C}$  and the supernatant was collected and added into 96-well plates. Final reaction buffer (50  $\mu\text{L}$ ) and caspase-3 colorimetric substrate (Ac-DEVDpNA 5  $\mu\text{L}$ ) were then added to each well. The plates were incubated at 37  $^{\circ}\text{C}$  for 2 h, and the optical density was measured at 405 nm with a plate reader (SpectraMax).

**Annexin V-FITC/PI (propidium iodide) staining**

The number of HeLa cell apoptotic events induced by the gold complexes was investigated using Annexin V and PI staining according to the manufacturer's protocol for the Dead Cell Apoptosis Kit with Annexin V-FITC and PI (V13242, Thermo Fisher), and analysed by flow cytometry (Thermo Fischer). Briefly, HeLa cells ( $1 \times 10^5$  cells/mL) in a 6 well plate were incubated with  $IC_{50}$  concentrations of the gold complexes for 48 h. After incubation, the cells were harvested and washed with PBS then suspended in 100  $\mu\text{L}$  Annexin V binding buffer (2.5 mM  $\text{CaCl}_2$ , 140 mM NaCl, 10 mM HEPES/NaOH, pH 7.4) 5  $\mu\text{L}$  each of Annexin V and 1  $\mu\text{L}$  of PI (100  $\mu\text{g}/\text{mL}$ ) were added and the cells were incubated for 15 min at room temperature. 10000 cells from each sample were analysed immediately by flow cytometric analysis (BD Accuri C6).

**Conflicts of interest**

There are no conflicts to declare.

**Acknowledgements**

The authors acknowledge the Micro Nano Research Facility (M NRF), RMIT University for providing the facilities to carry out these experiments.

**References**

1. T. Marzo, D. Cirri, C. Gabbiani, T. Gamberi, F. Magherini, A. Pratesi, A. Guerri, T. Biver, F. Binacchi, M. Stefanini, A. Arcangeli and L. Messori, *ACS Med. Chem. Lett.*, 2017, **8**, 997-1001.
2. A. De Nisi, C. Bergamini, M. Leonzio, G. Sartor, R. Fato, M. Naldi, M. Monari, N. Calonghi and M. Bandini, *Dalton Trans.*, 2016, **45**, 1546-1553.
3. T. Zou, C. T. Lum, C. N. Lok, J. J. Zhang and C. M. Che, *Chem. Soc. Rev.*, 2015, **44**, 8765-8942
4. B. Bertrand and A. Casini, *Dalton Trans.*, 2014, **43**, 4209-4219.
5. M. J. McKeage, L. Maharaj and S. J. Berners-Price, *Coord. Chem. Rev.*, 2002, **232**, 127-135.
6. M. A. Bennett, S. K. Bhargava, K. D. Griffiths, G. B. Robertson, W. A. Wickramasinghe and A. C. Willis, *Angew. Chem. Int. Ed. Engl.*, 1987, **26**, 258-260.
7. J. Forestier, *J. Lab. Clin. Med.*, 1935, **20**, 827-840.
8. <http://clinicaltrials.gov/ct2/show/NCT01419691>
9. C. K. Mirabelli, R. K. Johnson, D. T. Hill, L. F. Faucette, G. R. Girard, G. Y. Kuo, C. M. Sung and S. T. Crooke, *J. Med. Chem.*, 1986, **29**, 218-223.
10. S. Tian, F. M. Siu, S. C. F. Kui, C. N. Lok and C. M. Che, *Chem. Commun.*, 2011, **47**, 9318-9320.
11. A. Bindoli, M. P. Rigobello, G. Scutari, C. Gabbiani, A. Casini, A. and L. Messori, *Coord. Chem. Rev.*, 2009, **253**, 1692-1707.
12. A. De Luca, C. G. Hartinger, P. J. Dyson, M. L. Bello and A. Casini, *J. Inorg. Biochem.*, 2013, **119**, 38-42.
13. Ü. A. Laskay, C. Garino, Y. O. Tsybin, L. Salassa and A. Casini, *Chem. Commun.*, 2015, **51**, 1612-1615.
14. A. de Almeida, B. L. Oliveira, J. D. Correia, G. Soveral and A. Casini, *Coord. Chem. Rev.*, **257**, 2689-2704.
15. H. Scheffler, Y. You and I. Ott, *Polyhedron*, 2010, **29**, 66-69.
16. M. J. McKeage, S. J. Berners-Price, P. Galetti, R. J. Bowen, W. Brouwer, L. Ding, L. Zhuang and B. C. Baguley, *Cancer Chemother. Pharmacol.*, 2000, **46**, 343-350.
17. J. L. Hickey, R. A. Ruhayel, P. J. Barnard, M. V. Baker, S. J. Berners-Price and A. Filipovska, *J. Am. Chem. Soc.*, 2008, **130**, 12570-12571.
18. M. Serratrice, M. A. Cinellu, L. Maiore, M. Pilo, A. Zucca, C. Gabbiani, A. Guerri, I. Landini, S. Nobili, E. Mini and L. Messori, *Inorg. Chem.*, 2012, **51**, 3161-3171.
19. L. Maiore, M. A. Cinellu, E. Michelucci, G. Monetti, S. Nobili, I. Landini, E. Mini, A. Guerri, C. Gabbiani and L. Messori, *Inorg. Biochem.*, 2011, **105**, 230-237.
20. R. C. Bott, P. C. Healy and G. Smith, *Polyhedron*, 2007, **26**, 2803-2809.
21. P. J. Alonso, E. Cerrada, J. Garin, M. C. Gimeno, A. Laguna, M. Laguna and P. G. Jones, *Synth. Met.*, 1993, **56**, 1772-1776.
22. S. S. Zaleskiy, A. E. Sedykh, A. S. Kashin and V. P. Ananikov, *J. Am. Chem. Soc.*, 2013, **135**, 3550-3559.
23. D. Schneider, O. Schuster and H. Schmidbaur, *Dalton Trans.*, 2005, 1940-1947.
24. N. C. Baenziger, W. E. Bennett and D. M. Soborofe, *Acta Crystallogr.*, 1976, **B32**, 962-963.
25. G. Bandoli, D. A. Clemente, G. Marangoni and L. Cattalini, *J. Chem. Soc., Dalton Trans.*, 1973, 886-889.
26. R. J. Staples, C. King, M. N. I. Khan, R. E. P. Winpenny, J. P. Fackler Jr., *Acta Cryst.*, 1993, **49**, 472-475.

27. M. Patra, T. Joshi, V. Pierroz, K. Ingram, M. Kaiser, S. Ferrari, B. Spingler, J. Keiser and G. Gasser, *Chem. Eur. J.*, 2013, **19**, 14768-14772.
28. D. Gerlier and N. Thomasset, *J. Immunol. Methods.*, 1986, **94**, 57-63.
29. S. Nath and G. R. Devi, *Pharmacol. Thera.*, 2016, **163**, 94-108.
30. L. Sun, G. Li, X. Chen, Y. Chen, C. Jin, L. Ji and H. Chao, *Sci. Rep.*, 2015, **5**, 14837.
31. H. Huang, P. Zhang, H. Chen, L. Ji and H. Chao, *Chem. Eur. J.*, 2015, **21**, 715-725.
32. S. Sant, and P. A. Johnston, *Drug Discov. Today Technol.*, 2017, **23**, 27-36.
33. P. Friedl and K. Wolf, *Nat. Rev. Cancer*, 2003, **3**, 362-374.
34. L. Cattaruzza, D. Fregona, M. Mongiat, L. Ronconi, A. Fassina, A. Colombatti and D. Aldinucci, *Int. J. Cancer*, 2011, **128**, 206-215.
35. T. S. Reddy, S. H. Privér, N. Mirzadeh and S. K. Bhargava, *J. Inorg. Biochem.*, 2017, **175**, 1-8.
36. H. Yamaguchi and J. Condeelis, *Biochim. Biophys. Acta*, 2007, **1773**, 642-652.
37. D. Mustacich and G. Powis, *Biochem. J.*, 2000, **346**, 1-8.
38. J. Wang, M. Kobayashi, K. Sakurada, M. Imamura, T. Moriuchi and M. Hosokawa, *Blood*, 1997, **89**, 2480-2487.
39. G. L. Parrilha, K. S. Ferraz, J. A. Lessa, K. N. de Oliveira, B. L. Rodrigues, J. P. Ramos, E. M. Souza-Fagundes, I. Ott and H. Beraldo, *Eur. J. Med. Chem.*, 2014, **84**, 537-544.
40. T. S. Reddy, S. H. Privér, N. Mirzadeh and S. K. Bhargava, *Eur. J. Med. Chem.*, 2018, **145**, 291-301.
41. R. McCall, M. Miles, P. Lascuna, B. Burney, Z. Patel, K. J. Sidoran, V. Sittaramane, J. Kocerha, D. A. Grossie, J. L. Sessler, K. Arumugam and J. F. Arambula, *Chem. Sci.*, 2017, **8**, 5918-5929.
42. R. Rubbiani, S. Can, I. Kitanovic, H. Alborzinia, M. Stefanopoulou, M. Kokoschka, S. Monchgesang, W.S. Sheldrick, S. Wöfl and I. Ott, *J. Med. Chem.*, 2011, **54**, 8646-8657.
43. O. Rackham, S. J. Nichols, P. J. Leedman, S. J. Berners-Price and A. Filipovska, *Biochem. Pharmacol.*, 2007, **74**, 992-1002.
44. N. S. Jamaludin, Z. J. Goh, Y. K. Cheah, K. P. Ang, J. H. Sim, C. H. Khoo, Z. A. Fairuz, S. N. B. A Halim, S. W. Ng, H. L. Seng and E. R. Tiekink, *Eur. J. Med. Chem.*, 2013, **67**, 127-141.
45. A. G. Porter and R. U. Janicke, *Cell Death Differ.*, 1999, **6**, 99-104.
46. S. Nagata, *Exp. Cell Res.*, 2000, **256**, 12-18.
47. H. J. Lucas and E. R. Kennedy, *Org Synth, Coll. Vol. III*, Wiley: New York, 1955, 482.
48. R. Uson, A. Laguna and M. Laguna, *Inorg. Synth.*, 1989, **26**, 85-91.
49. A. Adé, E. Cerrada, M. Contel, M. Laguna, P. Merino and T. Tejero, *J. Organomet. Chem.*, 2004, **689**, 1788-1795.
50. C. Decker, W. Henderson and B. K. Nicholson, *J. Chem. Soc., Dalton Trans.*, 1999, 3507-3513.
51. SMART software ver. 5.625 for the CCD Detector System, Bruker AXS Inc.: Madison, WI, 2001.91
52. SAINTPLUS software ver. 6.22 for the CCD Detector System, Bruker AXS Inc.: Madison, WI, 2001.
53. R. H. Blessing, *Acta Crystallogr.*, 1995, **A51**, 33-38.
54. G. M. Sheldrick, SHELXTL, ver. 2013/4, Universität Göttingen, Germany, 2013.
55. G. M. Sheldrick, *Acta Crystallogr.*, 2008, **A64**, 112-122.

# Gold(I) and Gold(III) Phosphine Complexes: Synthesis, Anticancer Activities Towards 2D and 3D Cancer Models, and Apoptosis Inducing Properties

T. Srinivasa Reddy, Steven H. Privér, Vijay V. Rao, Nedaossadat Mirzadeh,\* Suresh K. Bhargava\*

Here in we report the synthesis of gold(I), gold(III) of tris(4-methoxyphenyl)phosphine and tris(2,6-dimethoxyphenyl)phosphine and their anticancer activity towards 2D and 3D cancer models.

